EUROPEAN JOURNAL OF CANCER 47 (2011) 479–490

available at www.sciencedirect.com

ScienceDirect

journal homepage: www.ejconline.com

A model of vascular tumour growth in mice combining longitudinal tumour size data with histological biomarkers

Benjamin Ribba [a,*], *Emmanuel Watkin* [b,c,d], *Michel Tod* [b,e,f], *Pascal Girard* [b,e,j], *Emmanuel Grenier* [a,g], *Benoît You* [b,e,h], *Enrico Giraudo* [i], *Gilles Freyer* [b,e,h]

[a] *INRIA, Project-team NUMED, Ecole Normale Supérieure de Lyon, 46 allée d'Italie, 69007 Lyon Cedex 07, France*
[b] *Université de Lyon, Lyon, F-69003, France*
[c] *Université Lyon 1, Faculté de Médecine Lyon-Est, Lyon F-69007, France*
[d] *Service d'Antomomie et Cytologie Pathologiques, Hôpital de la Croix Rousse, Hospices civils de Lyon, 69004 Lyon, France*
[e] *Université Lyon 1, EA3738 CTO, Faculté de Médecine Lyon-Sud, Oullins F-69600, France*
[f] *Pharmacie, Hôpital de la Croix Rousse, Hospices civils de Lyon, 69004 Lyon, France*
[g] *Ecole Normale Supérieure de Lyon, Unité de Mathématiques Pure et Appliquées (UMPA), 46 allée d'Italie, 69007 Lyon Cedex 07, France*
[h] *Service d'Oncologie Médicale, Centre Hospitalier Lyon-Sud, Hospices Civils de Lyon, 69310 Pierre-Bénite, France*
[i] *Laboratory of Transgenic Mouse Models, Institute for Cancer Research and Treatment, and Department of Oncological Sciences, University of Torino School of Medicine, Str. Prov. 142 Km 3, 95 10060 Candiolo, Torino, Italy*

ARTICLE INFO

Article history:
Received 14 June 2010
Received in revised form 8 September 2010
Accepted 8 October 2010
Available online 10 November 2010

Keywords:
Xenograft model antitumour assays
Models, theoretical
Models, statistical
Angiogenesis inducing agents
Histology

ABSTRACT

Optimising the delivery of antiangiogenic drugs requires the development of drug–disease models of vascular tumour growth that incorporate histological data indicative of cytostatic action. In this study, we formulated a model to analyse the dynamics of tumour progression in nude mice xenografted with HT29 or HCT116 colorectal cancer cells. In 30 mice, tumour size was periodically measured, and percentages of hypoxic and necrotic tissue were assessed using immunohistochemistry techniques on tumour samples after euthanasia. The simultaneous analysis of histological data together with longitudinal tumour size data prompted the development of a semi-mechanistic model integrating random effects of parameters. In this model, the peripheral non-hypoxic tissue proliferates according to a generalised-logistic equation where the maximal tumour size is represented by a variable called 'carrying capacity'. The ratio of the whole tumour size to the carrying capacity was used to define the hypoxic stress. As this stress increases, non-hypoxic tissue turns hypoxic. Hypoxic tissue does not stop proliferating, but hypoxia constitutes a transient stage before the tissue becomes necrotic. As the tumour grows, the carrying capacity increases owing to the process of angiogenesis. The model is shown to correctly predict tumour growth dynamics as well as percentages of necrotic and hypoxic tissues within the tumour. We show how the model can be used as a theoretical tool to investigate the effects of antiangiogenic treatments on tumour growth. This model provides a tool to analyse tumour size data in combination with histological biomarkers such as the percentages of hypoxic and necrotic tissue and is shown to be useful for gaining insight into the effects of antiangiogenic drugs on tumour growth and composition.

* *Corresponding author*: Tel.: +33 4 72 72 84 17; fax: +33 4 72 72 84 80.
E-mail address: benjamin.ribba@inrialpes.fr (B. Ribba).
[j] Present address: Merck Serono, 9 ch des Mines, CH1202 Geneva, Switzerland.
0959-8049/$ - see front matter © 2010 Elsevier Ltd. All rights reserved.
doi:10.1016/j.ejca.2010.10.003

1. Introduction

Cancer therapy research has recently moved towards the development and use of targeted drugs that act on specific processes involved in neoplastic progression. Angiogenesis is a critical process in tumour development, disease progression and metastatic spread,[1] and the last 10 years have seen the development of an increasing number of antiangiogenic agents.[2] In clinical trials, however, monotherapy with antiangiogenic agents has not yet been shown to increase patient survival. Treatment combining such drugs with conventional cytotoxic therapy has yielded beneficial effects, but the mechanisms of these effects are still poorly understood.

One difficulty in antiangiogenic drug development is the proper evaluation of drug efficacy. Reliance on the conventional end-point of tumour volume is problematic, since antiangiogenic drugs are cytostatic in action and do not directly induce tumour shrinkage.[3] Biological markers (biomarkers) from immunohistochemical analysis are currently used in preclinical studies, but no such biomarkers have been validated for clinical antiangiogenic therapy. Furthermore, because biomarkers are often measured at a single time point for all experimental subjects, the information they provide is incomplete.

Mathematical models that characterise and quantify the dynamics of tumour progression and response to anticancer treatments can provide valuable insights for cytostatic drug development. Models that integrate tumour size alone have been well established. A standard and robust model, namely the modified Gompertz model, has been proposed to predict tumour growth inhibition in mice treated with chemotherapeutic compounds.[4,5] Additional studies have focused on the translation of these modelling results in mice to gain clinical insights into optimal drug delivery.[6] The development of simple phenomenological models, based on rich clinical data sets, has led to significant recent achievements. In particular, models linking tumour size in patients to survival have been proposed.[7,8]

Numerous biomathematical and biophysical models have been developed to better understand the complex mechanisms involved in the process of angiogenesis, its role in tumour growth and the consequences of its inhibition.[9–12] However, due to their complexity and the large number of parameters they integrate, these theoretical models are often limited in terms of applications. Hahnfeldt and coworkers have proposed a simple extension of the classical Gompertz model to take into account the process of angiogenesis.[13] In their model, the tumour limiting size, or 'carrying capacity', is the result of competition between pro- and anti-angiogenic molecules. This model has been successfully fitted to volume data for Lewis lung carcinoma subcutaneously xenografted in mice either treated or not with different antiangiogenic compounds.

To provide information relevant to antiangiogenic drug therapy, models of tumour dynamics must incorporate, in addition to tumour size, biomarkers that reflect the action of cytostatic agents. The increasing availability of computational resources has enabled researchers to extend simple tumour growth models into complex and validated drug–disease models. Bueno and colleagues[14] proposed a semi-mechanistic model of the tumour growth inhibitory effect of an anticancer compound integrating molecular biomarkers from the TGF-β pathway. Gorelik and coworkers[15] used immunohistochemical data assessed through xenograft biopsies to refine the evaluation of a mechanistic vascular tumour growth model.[16] New studies aimed at modelling the dynamics of angiogenesis molecular markers such as circulating vascular endothelial growth factor (VEGF) under antiangiogenic treatments are in preparation.[17]

In the present paper, we used longitudinal and histological data collected from mice injected with human colorectal carcinoma cells. We formulated a model of vascular tumour growth combining these two types of data. The model, formulated as a system of ordinary differential equations, contains four variables describing the evolution of non-hypoxic, hypoxic and necrotic tissue. A fourth unobserved variable regulates tumour growth owing to the process of tumour angiogenesis. We validated the model with observations of tumour size and percentages of necrotic and hypoxic tissue within the tumour, considered as histological biomarkers. An application of the model is demonstrated by simulating the efficacy of an antiangiogenic treatment.

2. Materials and methods

2.1. Cell culture

HT29 and HCT116 human colorectal adenocarcinoma cells were grown in advance in a rich environment (Dulbecco's Modified Eagle's Medium) containing foetal calf serum (10%), penicillin and streptomycin (1%).

2.2. Animals

Female athymic nude mice, 6–8 weeks of age ($n = 30$; average weight 20 g), were obtained from Harlan, Gannat, France. Mice were maintained in cages with filter paper covers, sterilised food and bedding and acidified water. All animal experiments were conducted in accordance with the *Guide for the Care and Use of Laboratory Animals* (NIH publication #85-23, revised 1985).

2.3. In vivo tumour growth experiments

About 6×10^6 cells in 100 μL of phosphate-buffered saline were injected into the right flank of each mouse; 15 mice were injected with HT29 cells, and 15 were injected with HCT116 cells. We examined and collected data from each mouse once every 2–3 days for up to 7 weeks.

2.4. Tumour size data collection

At each observation, we used a slide calliper to measure the diameter of each tumour that was visible to the eye. Two perpendicular diameter measurements (denoted L for the largest and l for the smallest) were taken for each mouse. The

measure of tumour size we chose to analyse was the mean tumour diameter $\left(\frac{L+l}{2}\right)$ rather than the commonly used approximation of tumour volume through the ellipsoid formula $\left(\frac{Ll^2}{2}\right)$. The following considerations motivated our choice: (i) diameters are actually measured, whereas volume calculations manipulate diameter data, compounding the influence of errors of measurement. (ii) The actual shape of each tumour is not similar to an ellipsoid. In particular, the third dimension (height) is generally much smaller than the two others (see for example Fig. 1C for a typical view of tumour shape 35 d after cell injection). (iii) Recent studies aimed at modelling tumour growth in clinical settings and predicting survival in clinical trials use tumour diameter as tumour size data.[7,8,18] Finally, even if the common way to analyse tumour growth in xenografted mice involves the use of the approximated volume, there is no clear reason to believe that the use of the mean diameter could not be a reliable parameter for describing the tumour growth dynamics in terms of tumour size.

2.5. *Euthanasia and tumour dissection*

Two or three mice from each group (HT29 or HCT116) were euthanised each week by intraperitoneal pentobarbital injection. Tumours were dissected and halved. One half was fixed in buffered formalin at a concentration of 10%, and the other was frozen in liquid nitrogen. It is important to mention that selection of animals for euthanasia was not random. There was a tendency to select the mice with the largest tumours to be euthanised first.

2.6. *Immunohistochemistry*

The tumour-half fixed in formalin was embedded in paraffin. Immunohistochemistry (IHC) analysis was carried out on 10-μm-thick slices using the Ventana Discovery automated system.

To identify hypoxic tissue, we used the antibody anti-CA IX (Carbonic Anhydrase IX). CA IX is a stable protein from the

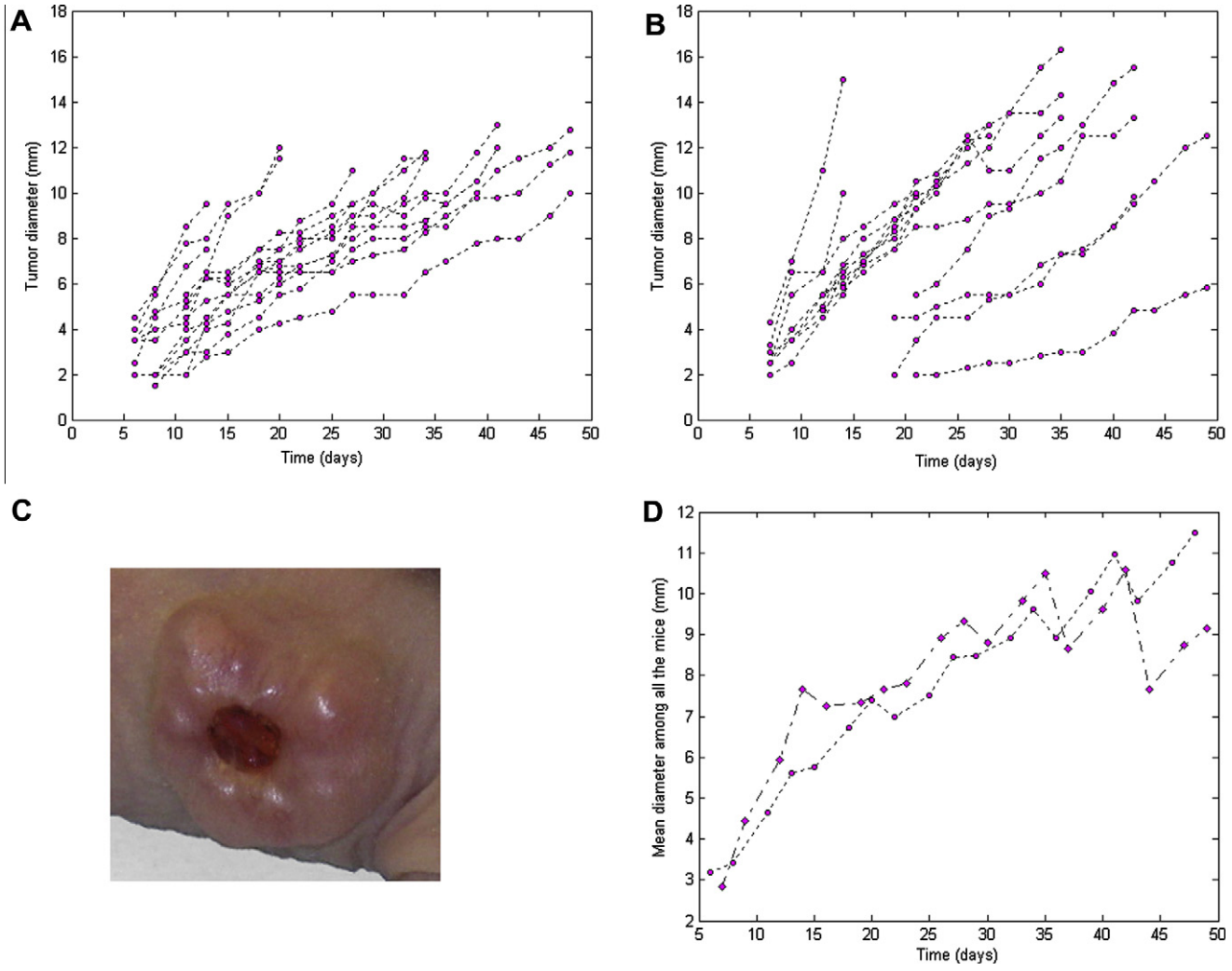

Fig. 1 – Tumour growth. (A) Plots of individual tumour growth (mean of two perpendicular diameters) in 15 mice injected with HT29 versus time after cell implantation. (B) Plots of individual tumour growth (mean of two perpendicular diameters) in 15 mice injected with HCT116 versus time after cell implantation. (C) Typical view of a tumour 35 days after a subcutaneous injection of 6 million HT29 (human colorectal adenocarcinoma) cells. (D) Mean tumour growth curves for each group: HT29 (circles) and HCT116 (diamonds).

cell membrane whose transcription is induced by HIF-1α (hypoxia inducible factor) in response to hypoxic stress.[19] IHC staining using anti-CA IX resulted in colouration of cell membranes expressing the protein. Using a microscope imaging station, we delineated the contour of the coloured area and estimated the corresponding surface area using HistoLab software (MicroVision Systems, Evry, France). However, this surface encompasses not only the hypoxic tissue but also the necrotic tissue located in the central part of the tumour. Staining the same slice with haematoxylin allowed us to delineate the contour of the necrotic tissue. Indeed, with this staining, significant morphological differences between the necrotic tissue and the viable tissue became apparent. Finally, we delineated the contour of the whole tumour slice to estimate the entire surface area. Fig. 2C shows a tumour slice in which non-hypoxic, hypoxic and necrotic areas are highlighted with distinct colours.

To qualitatively assess the location of proliferating cells within the tumour, we used IHC staining against the Ki67 protein. This resulted in a brown colouration of cells undergoing their proliferation cycles.

2.7. *Modelling technique*

2.7.1. *Mixed-effects models*

The formulated vascular tumour growth model belongs to the category of mixed-effect models. Mixed-effects or population models take into account different levels of variability among individuals.[20] In their general form, such models can be written as follows:

$$y_{ij} = f(x_{ij}, \phi_i) + g(x_{ij}, \phi_i)\varepsilon_{ij}, \quad 1 \leqslant i \leqslant N; \quad 1 \leqslant j \leqslant n_i$$

where N is the number of individuals, n_i the number of observations for individual i, x the regression variable (e.g. time) and y the observations. The term f is the structural model. Our mathematical model for tumour growth is expressed as systems of ordinary differential equations (ODE) relying on the expression of a variation in the analysed measurement (e.g. tumour size) in an infinitesimal time step.

The residual error is $g(x_{ij}, \phi_i)\varepsilon_{ij}$, where $\varepsilon_{ij} \sim N(0, \sigma^2)$. In the following, we will consider constant error models $g(x_{ij}, \phi_i) = 1$.

The individual parameters (φ_i) can be defined as follows:

$$\phi_i = h(\mu + \eta_i), \quad \eta_i \sim N(0, \Omega), \quad i = 1, \ldots, N,$$

where μ is a p-vector of fixed population parameters (i.e. $h(\mu)$ is the median value across individuals for each of the p parameters), η_i is a p-vector of random effects, Ω is the $p \times p$ variance-covariance matrix of the random effects and h is some predefined transformation. Here, we assume that the individual parameters are log-normally distributed (i.e. $h(u) = e^u$). We assume potential correlations between the random effects (Ω is a full matrix).

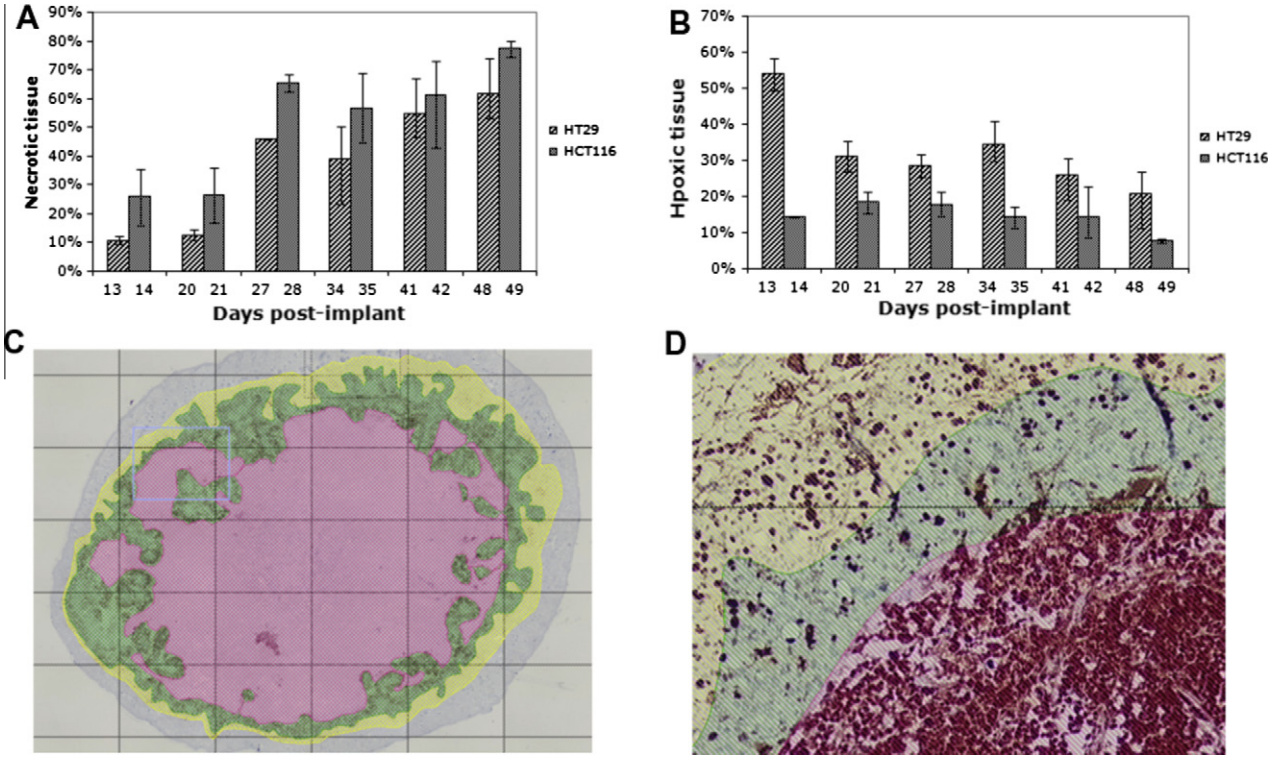

Fig. 2 – Changes in tumour biology over time. (A) Percentage of necrotic tissue. (B) Percentage of hypoxic tissue. (C) A typical view of a tumour slice after IHC staining with both anti-CA IX to reveal the hypoxic tissue (green area) and haematoxylin to highlight the necrotic tissue (pink area). The full tumour contour is delineated by using a microscope imaging station. This enables localisation of the non-hypoxic tissue area (in yellow). The three areas are automatically calculated by the software HistoLab. (D) Typical view of a tumour sample marked with Ki67 resulting in brown colouration of cells undergoing the proliferation cycle. We performed this test to verify that the hypoxic tissue (green area) was likely to be a proliferating tissue.

The unknown set of parameters in the model is then:

$$\theta = (\mu, \Omega, \sigma^2).$$

The likelihood function related to this problem can be written as follows:

$$L(\theta, y) = \prod_{i=1}^{N} L_i(\theta, y_i)$$

with

$$L_i(\theta, y_i) = \int p(y_i, \eta_i, \theta)\, d\eta_i = C \int \sigma^{-n_i} |\Omega|^{-1/2} e^{-\frac{1}{2\sigma^2}\|y_i - f(x_i, \phi_i)\|^2 - \frac{1}{2}\eta_i \Omega^{-1} \eta_i} d\eta_i$$

For our model, we extended the general formulation to multi-response models, as we analysed several variables: tumour size as well as histological biomarkers (necrotic and hypoxic tissue).

In this case, the global likelihood function is the unbalanced sum of all likelihood functions written for each observation.

If f is non-linear with respect to the random effects, the likelihood function cannot be easily computed and maximised. Several methods can help solve this problem. The most intuitive is analysing the data from each individual separately, but this requires a large number of observations per individual. A recent novel approach, however, is the SAEM algorithm (Stochastic Approximation of the EM algorithm), which can be used to calculate the maximum likelihood, without any approximation of the likelihood function, and to estimate population (θ) and individual (φ_i) parameters.[21] We used Monolix 2.4 to solve this issue and estimate the model parameters.

2.7.2. *Matching the model outputs with the histological data*

The model we developed includes three variables: the non-hypoxic proliferative tissue (*P*), hypoxic tissue (Q) and necrotic tissue (*N*) expressed in millimetres. The sum of the three variables ($P + Q + N = P^*$) was directly matched to the measured mean tumour diameters. The model variables were combined to calculate the percentages of hypoxic tissue ($\frac{Q}{P^*} \times 100$) and necrotic tissue ($\frac{N}{P^*} \times 100$). However, as the percentages of necrotic and hypoxic tissue were previously quantified as surface areas, a modification of those data was applied to match the model outputs. The percentage of necrotic tissue was calculated by taking the square root of the ratio of the necrotic area to the whole tumour area and then multiplied by 100. This value was then directly compared to $\frac{N}{P^*} \times 100$.

To retrieve the percentage of hypoxic tissue, we first applied a square root to the ratio of hypoxic area to the whole tumour area. As the hypoxic area encompassed the necrotic core, we then removed the percentage of necrotic tissue previously calculated, and finally multiplied by 100. The remaining value was directly compared to $\frac{Q}{P^*} \times 100$.

2.8. *Model building and diagnosis*

The log-likelihood (*LLH*) value (actually $-2 \times LLH$) is generally used to select the best model from among multiple models. However, as a model with more parameters will generally produce a better fit as it has more degrees of freedom, a penalty term can be introduced into the likelihood function to account for the number of parameters. Examples of criterion functions that include such penalty terms are the Akaike information criterion (*AIC*):

$$AIC = -2 \times LLH + 2 \times n,$$

where n is the number of free parameters to be estimated, and the Bayesian information criterion (*BIC*):

$$BIC = -2 \times LLH + \log(k),$$

where k is the sample size.

Selection between models was based on the three criterion functions, i.e. $-2 \times LLH$, *AIC* and *BIC* values, as well as goodness of fit, residual plots and precision of parameter estimates as relative standard errors.

We calculated ε-shrinkage and η-shrinkage to analyse the degree of shrinkage of individual predictions towards the observations.[22] In case of low shrinkage (<20%), individual predictions were considered reliable for model diagnostics.

Simulation-based diagnostics were assessed through visual predictive check, which is based on a graphical comparison between the observed data and the simulated data (using population parameters and both inter-individual and residual variability).[22]

3. Results

3.1. *Presentation of data*

Fig. 1A and B shows the changes in individual tumour diameter (mean of two perpendicular diameters) over time in two groups of mice (HT29 and HCT116 xenograft mice). There was large variability among individual animals, in particular among HCT116 xenograft mice (Fig. 1B). However, there was no significant difference in tumour growth between the two groups. We thus analysed all data taken together and considered the cell line as a potential categorical model covariate.

Fig. 2A and B presents the percentage of necrotic and hypoxic tissues in HT29 and HCT116 tumours assessed with the previously described method after euthanasia. The percentage of hypoxic tissue was significantly higher in HT29 tumours than in HCT116 tumours ($p < 0.001$ for the mean over all time points – calculated with a Wilcoxon test [23]). The opposite trend was observed for the necrotic tissue percentage, but this difference was not significant. Fig. 2C shows the colouration of a tumour slice stained with both anti-CA IX and haematoxylin to reveal the hypoxic and necrotic tissues, respectively. As noted above, the percentages of hypoxic and necrotic tissues were assessed from these images using a microscope imaging station equipped with the software HistoLab. Finally, Fig. 2D shows the overlapping of a part of tumour slice marked as in 2C and the same area marked with Ki67. Immunostaining with Ki67 reveals the cells progressing through the cell cycle (nuclei of proliferating cells are coloured in brown). These types of images were produced to analyse the proliferation activity of cells in the hypoxic tissue.

3.2. *Model of vascular tumour growth*

We developed a model in which the tumour spheroid is composed of non-hypoxic, hypoxic and necrotic cells. The model

is composed of four ordinary differential equations (ODE), and the derivatives of our variables are expressed as balances between production and elimination terms, as in classical compartment models. The model is written without taking into account any spatiality dimensions of the tumour. The variables refer to quantities of tissue of different types (non-hypoxic, hypoxic and necrotic), expressed in millimetres. This is equivalent to the assumption that converting the information of the actual three-dimensional tumour (whose variables would be expressed in mm^3) to information in a single dimension (mm) does not have a major influence on the analysis of the system dynamics.

We ran the estimation procedure for three types of outputs (tumour diameter, percentage of necrotic tissue and percentage of hypoxic tissue) using Monolix software.[k]

The basic assumption underlying the model structure can be summarised as follows: proliferative non-hypoxic tissue (P) proliferates according to a generalised-logistic equation, where the maximal size is a variable of the model called carrying capacity (K). A fraction of proliferative tissue becomes hypoxic (Q). Hypoxic tissue does proliferate and degrades into necrotic tissue (N). As the tumour size grows, the carrying capacity increases to account for the process of angiogenesis.

Slightly different model structures were tested and compared to the basic structure. In particular, the addition of a constant rate of transfer from the proliferative compartment directly to the necrotic compartment did not improve the fits (resulting in a BIC increase of 39 points), nor did addition of a constant rate of elimination from the necrotic tissue compartment (BIC increase of 42 points). The latter may seem counterintuitive, since it is likely that cell loss is present and is relevant to tumour growth. In models integrating this degradation term, the parameter was estimated at a small value (around 5×10^{-4}) with a high standard error (i.e. the estimated value is not significantly different from 0). The problem was partially solved by fixing the mean value of this parameter (to a small value) and by only estimating its variability. However, this again resulted in poorer fit (a BIC increase of 39 points compared with the basic model structure). In conclusion, a degradation term from the necrotic compartment was not taken into account in the final model structure. We could, however, find an explanation for these results. In the particular case of subcutaneous xenografts, the necrotic tissue seems wholly trapped in the central core of the tumour as shown Fig. 1C. In other words, even if necrotic tissue degrades, it has no way to escape the necrotic core.

Finally, the removal of the proliferation term in the hypoxic tissue did provide results comparable to those of the basic structure (BIC decrease of 7 points but AIC increase of 4 points). However, using the Ki67 staining, we found strong evidence to support the fact that hypoxic cells did proliferate, as shown in Fig. 2B. Due to this evidence, we maintained a proliferative term in the hypoxic tissue.

We then adjusted the model structure by attempting a modulation of transfer coefficients from tissue compartments. Hypoxic stress was used as the modulator term and was represented by the ratio between the full tumour size and the carrying capacity (as in the growth limitation of the logistic growth term). The log-likelihood ($-2 \times LLH$) was used to compare the models, as the number of parameters was unchanged. Only the modulation of the transfer coefficient from non-hypoxic to hypoxic tissue resulted in a reduction of the objective function ($-2 \times LLH$ decrease of 13 points).

The resulting model is as follows:

$$\begin{cases} \frac{dP}{dt} = \lambda_P P(1-s^\alpha) - k_{PQ} P s^\alpha, \quad P(t=0) = P_0 \\ \frac{dQ}{dt} = k_{PQ} P s^\alpha + \lambda_Q Q(1-s^\alpha) - k_{QN} Q, \quad Q(t=0) = 0 \\ \frac{dN}{dt} = k_{QN} Q, \quad N(t=0) = 0 \\ \frac{dK}{dt} = b P^*, \quad K(t=0) = K_0 \\ P^* = P + Q + N \quad \text{and} \quad s = \frac{P^*}{K} \end{cases},$$

where P^* denotes the total number of cells in the tumour and s the hypoxic stress regulating the logistic growth of the non-hypoxic and hypoxic tissues and modulating the transfer between these two types of tissue. The exponent α, which reflects the effect of the hypoxic stress on the variables' evolution, was not estimated. It was fixed to a low value ($\alpha = 0.1$) for which the logistic proliferation term is equivalent to a Gompertz law, classically used to model tumour growth. Since cells were grown in a rich medium prior to their injection, we assumed that cells were neither hypoxic nor necrotic at the time of xenograft ($t = 0$). Fig. 3 shows a schematic illustration of the model as well as an illustration of its simulation and the evolution of the model variables.

Inter-animal variability in the model parameters (P_0, K_0, λ_P, k_{PQ}, λ_Q, k_{QN}, b) was assumed to be log-normally distributed, and mouse-specific estimates are given as follows, e.g. for P_0:

$$P_{0i} = P_0 e^{\eta_i^{P_0}}$$

where P_0 is the typical value for the population (mean value) and $\eta_i^{P_0}$ is an inter-animal random effect that follows a normal distribution with mean 0 and variance $\omega_{P_0}^2$.

Finally, the cell line was evaluated as a categorical covariate. We tested the inclusion of this covariate on all the parameters following a stepwise-backward method.[24] As a result, the cell line was successfully integrated in the transfer coefficient from hypoxic to necrotic compartments (k_{QN}) and in the parameter linking the increase in carrying capacity to the whole tumour size (b).

In consequence, the parameters k_{QN} and b each have two mean values according to the cell line (HT29 or HCT116). This can be written as follows:

$$k_{QN}^{HCT116} = k_{QN}^{HT29} e^{\beta_{k_{QN}}} \quad \text{and} \quad b^{HCT116} = b^{HT29} e^{\beta_b}.$$

The mean growth rate for the non-hypoxic layer of the tumour spheroid was estimated at 1.24 per day, which corresponds to a cell cycle mean duration of less than 24 h, which seems biologically consistent. Interestingly, the growth rate of the hypoxic tissue was found to be slightly higher (1.43 per day). It is clear from Fig. 2D that density of cells marked with Ki67 in the hypoxic tissue (green area) is not substantially lower than in the non-hypoxic tissue (yellow area). However, there is no rational reason to think that proliferation in the hypoxic tissue would be higher than in the

[k] http://www.monolix.org

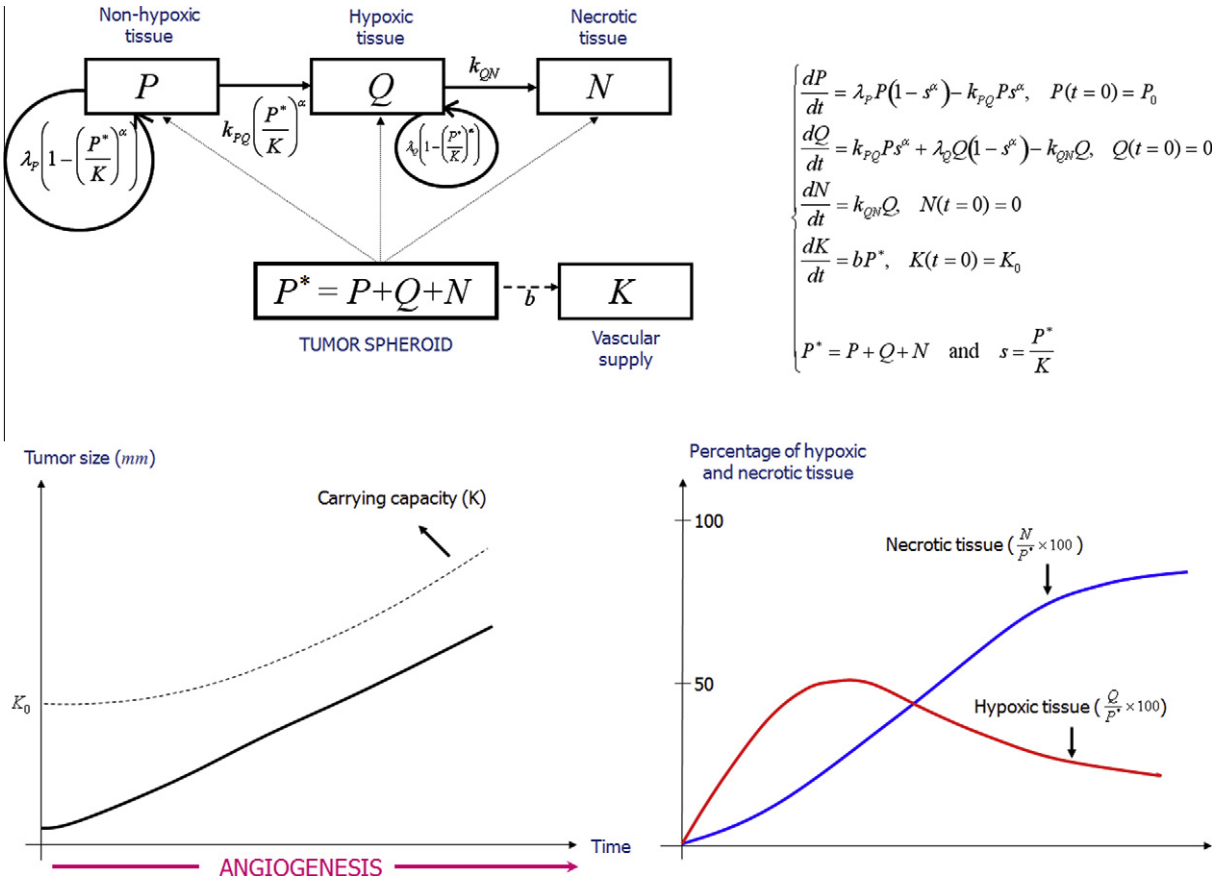

Fig. 3 – Schematic description of the mathematical models: model diagram, equations and evolution of the main model variables and outputs.

non-hypoxic tissue. We may try to explain this paradoxical finding by attributing it to the selection bias for mouse euthanasia. Indeed, because the animals with the most aggressive tumours were euthanised first, as time progressed, the remaining animals tended to be characterised by slower growing tumours. Consequently, while the necrotic tissue percentage is likely to gradually increase as tumours grow, there is potentially, in our dataset, an overestimation of the necrotic tissue percentages at the latest time points (animals euthanised latest). As in the model, necrosis is only generated from hypoxic tissue; this may imply an overestimation of the proliferation parameter in this compartment.

The mean rate of transfer from the non-hypoxic to the hypoxic compartment was 0.06 per day. We note, however, that this transfer is modulated by the hypoxic stress s, and the latter term is always <1 in the case of untreated tumours. The cell line was successfully introduced as a categorical covariate in the estimation of the transfer rate from hypoxic to necrotic tissue, k_{QN}. This parameter was estimated in the mean at 0.07 per day for tumours xenografted with HT29 cells, while it was 0.2 per day for HCT116 tumours. In light of these results, it is likely that resistance to hypoxic stress is much greater in HT29 cells than in HCT116 cells. This is consistent with our dataset, in which the percentage of hypoxic tissue was significantly higher in tumours generated from HT29 xenografts than in those generated from HCT116 xenografts (see Fig. 2B).

The cell line was also introduced as a categorical covariate in the estimation of b, the rate of increase of the carrying capacity. This parameter was estimated in the mean at 0.03 per day for HT29 tumours, while it was 0.05 per day for HCT116 tumours. This suggests that HT116 tumours may have higher angiogenic potential compared with HT29 tumours.

Table 1 presents the parameter estimates of the model as mean values, standard deviation of random effects. Fig. 4 shows model diagnosis for the three outputs (tumour size, necrotic tissue percentage and hypoxic tissue percentage). In the first row, the individual predictions are represented versus the actual observations. In addition to the excellent individual predictions of tumour size, predictions of necrotic ($r^2 = 0.94$, $p < 0.001$) and hypoxic ($r^2 = 0.84$, $p < 0.001$) tissue percentages are correct. Given the inter-individual variation regarding the latter two outputs, it would be interesting to use a larger sample size to consolidate these findings. Visual predictive checks for the three outputs are shown in the second row. In these calculations, we took into account the euthanasia procedure and the bias that this may have implied. This was done by removing from the simulated population the 'virtual mice' carrying the largest tumours at the same time points and respecting the same proportions (number of mice removed versus the entire population at a given time point) as in the real experiment. This explains why the simulated mean growth curve tends to reach a saturation

Table 1 – Parameters are defined in the text. IAV, inter-animal variability expressed as percentage. Coefficients of variation (%) are shown in parentheses and are computed as the ratio between the standard error and the parameter estimate multiplied by 100. Shrinkage is expressed as percentage and refers to η-shrinkage for structural model parameters and ε-shrinkage for residual error model parameters.

Parameters	Description	Estimate	IAV	Shrinkage
P_0	Initial tumour size	0.32 mm (25)	99 (13)	6
K_0	Initial carrying capacity	10.4 mm (9)	52 (20)	2
λ_P	Growth rate for the non-hypoxic tissue	1.24 d^{-1} (11)	62 (12)	4
k_{PQ}	Transfer rate from non-hypoxic to hypoxic tissue compartment	0.06 d^{-1} (12)	46 (35)	3
λ_Q	Growth rate for the hypoxic tissue	1.43 d^{-1} (20)	65 (18)	1
k_{QN}^{HT29}	Transfer rate from hypoxic to necrotic tissue compartment for the HT29 cell line	0.07 d^{-1} (10)	61 (14)	
$\beta_{k_{QN}}$	Covariate (cell line) on parameter k_{QN} (exponential formulation)	1.07 (11)	–	
k_{QN}^{HCT116}	Transfer rate from hypoxic to necrotic tissue compartment for the HCT116 cell line	0.20 d^{-1}	–	
b^{HT29}	Rate of increase of carrying capacity for HT29 cell line	0.03 d^{-1} (30)	95 (11)	6
β_b	Covariate (cell line) on parameter b (exponential formulation)	0.5 (72)	–	
b^{HCT116}	Rate of increase of carrying capacity for HCT116 cell line	0.05 d^{-1}	–	
a_1	Error model parameter for the output 'tumour size' (exponential formulation)	0.09 (5)	–	1
a_2	Error model parameter for output 'necrotic tissue percentage' (exponential formulation)	0.12 (43)	–	18
a_3	Error model parameter for output 'hypoxic tissue percentage' (exponential formulation)	0.18 (41)	–	8

size. This feature can actually be also observed in the data (see Fig. 1D). In conclusion, the model is shown to correctly predict the simultaneous progression over time of tumour size and of two histological biomarkers: necrotic and hypoxic tissue percentages.

3.3. 3 Simulation of antiangiogenic treatment

We used our model as a theoretical tool to simulate the effect of antiangiogenic treatment. We considered two possible antiangiogenic effects: inhibition of vasculature formation and disruption of vasculature. Vasculature-inhibiting treatment was modelled by multiplying the growth parameter of the carrying capacity K by a constant positive factor smaller than one during the treatment period:

$$\begin{cases} \frac{dK}{dt} = b\gamma P^*, \quad \text{with} \begin{cases} 0 < \gamma < 1 & \text{during treatment} \\ \gamma = 1 & \text{otherwise} \end{cases} \\ K(t=0) = K_0 \end{cases}$$

Vasculature-disrupting treatment was modelled distinctly by adding an addition term to the equation. This term is negative during the treatment and null otherwise:

$$\begin{cases} \frac{dK}{dt} = bP^* - \xi K, \quad \text{with } \{ \xi > 0 \quad \text{during treatment} xi = 0 \quad \text{otherwise} \\ K(t=0) = K_0 \end{cases}$$

Fig. 5 presents tumour response to 10 d of treatment (from day 20 to day 30). The tumour growth model parameters were set to the mean parameters previously estimated. Parameters γ and ξ were set to arbitrary values $\gamma = \frac{1}{10}$ and $\xi = 0.1$ per day. With these parameter values, we observe two distinct behaviours. In the 'vessel inhibition' case, the carrying capacity almost ceases to increase during the treatment period, while in the 'vasculature disruption' case it strongly decreases due to the negative term in the equation (Fig. 5B). These two different behaviours result from the two previous equations. In fact, in the 'vessel inhibition' case, the carrying capacity's rate of increase can, at best, be reduced, but it always remains positive or null. In the 'vasculature disruption' case, the term ξK can become higher than the term bP^* during the treatment, leading $\frac{dK}{dt}$ to become negative and thus K to decrease.

As a consequence, tumour growth only slows down in the first case, whereas the tumour slightly regresses in the second case (Fig. 5A). The latter effect is due to the logistic terms regulating the tissue proliferation, which become negative when the carrying capacity (K) goes below the tumour size (P^*).

Regarding the histological markers, hypoxic tissue formation is increased in both treatment cases, since this process is mediated through the hypoxic stress $\frac{P^*}{K}$. However, as for the non-hypoxic tissue, proliferation in the hypoxic tissue is reduced due to hypoxia and may become negative in the 'vasculature-disrupting' case. This explains the seemingly paradoxical observation of a stronger decrease in hypoxic tissue percentage in the treatment cases compared with the untreated tumour (Fig. 5D). Finally, the percentage of necrotic tissue is increased in the treatment cases compared with the untreated case (Fig. 5C). The absolute size of the necrotic zone is actually smaller in treated tumours than in untreated tumours, but given that the size of treated tumours is smaller, the percentage of necrotic tissue appears larger.

We can conclude that only the 'vasculature-disrupting' effect may lead to tumour regression. In both treatment cases, the model predicts that treated tumours are characterised by

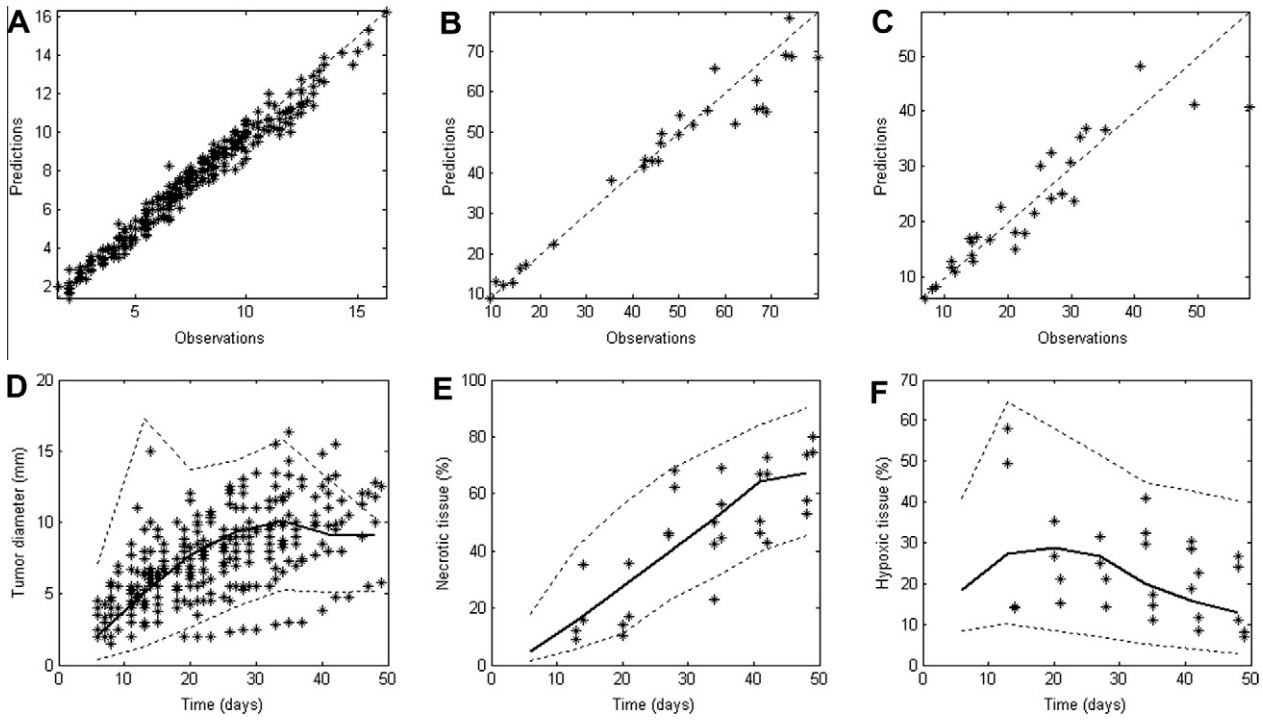

Fig. 4 – Semi-mechanistic model predictions. (A) Individual predictions (IPRED) of tumour size versus actual observation (OBS). The dotted line is the identity. (B) IPRED versus OBS graph for the necrotic tissue percentage. (C) IPRED versus OBS graph for the hypoxic tissue percentage. (D) Simulations of the semi-mechanistic model with 95% confidence interval (dotted lines) are shown together with tumour size data (visual predictive check). The continuous line shows model simulation using the population (mean) parameters. (E) Same as D for the percentage of necrotic tissue. (F) Same as D for the percentage of hypoxic tissue.

a smaller size, a larger necrotic tissue percentage and a lower hypoxic tissue percentage compared with untreated tumours. It is worthwhile to emphasise that in the model, the treatment does not directly cause necrotic tissue expansion. Rather, it mainly results in a direct elimination of non-hypoxic and hypoxic cells, which causes tumour size reduction, thus modifying the fraction of necrotic and hypoxic tissue.

Direct experimental validations of the assumptions are obviously warranted in order to turn the model into a practical tool for exploring different schedules for specific drugs.

4. Discussion

The nude mouse bearing subcutaneous human cancer cell xenografts is a preclinical model with many advantages. Induction and observation of tumours involve no surgical intervention, and the characteristics of the growing tumour are often similar to those in *in vitro* tumour models. The mice develop a fairly regular spheroid tumour structure within a few days. We analysed tumour size and IHC data obtained from 30 mice that were xenografted with either HT29 or HCT116 cell lines.

We built a semi-mechanistic model of spheroid growth reproducing the main features of tumour biology: proliferation, hypoxia and angiogenesis. The model integrates three types of tissue (non-hypoxic, hypoxic and necrotic) and is based on the following hypothesis: as the tumour grows, hypoxia develops within the spheroid and drives the formation of hypoxic tissue. Hypoxic tissues become in turn necrotic with a constant transfer rate. Depending on the whole tumour size, the carrying capacity, which also stands as the maximal tumour size, increases as a result of the process of angiogenesis. We carefully determined the best model structure by trying to add or remove biological components that appeared potentially relevant to us, e.g. direct transfer from non-hypoxic to necrotic tissue, elimination from the necrotic tissue compartment and modulation of the transfer constant by hypoxic stress. The final model is shown to correctly predict tumour size progression as well as the percentages of necrotic and hypoxic tissues despite individual variability among animals. Moreover, the inclusion of the cell line as a categorical covariate led us to generate a hypothesis on the main differences between these cell lines with respect to hypoxia resistance and intrinsic angiogenic potential. It was found that HT29 tumours might be more resistant to hypoxia compared with HCT116 tumours (rate of transfer from hypoxic to necrotic tissue was drastically lower in the case of HT29). Moreover, it was found that HCT116 tumours were characterised by a higher angiogenic potential. Note that the two parameter estimates (k_{QN} and b) were not correlated.

Our model is more complex than traditional models used to analyse tumour size. However, its formulation, based on compartments, is rather classical in the field of pharmacokinetic/pharmacodynamic (PK/PD) modelling. Its main innovation lies in its ability to integrate classical histological biomarkers such as those commonly retrieved in preclinical

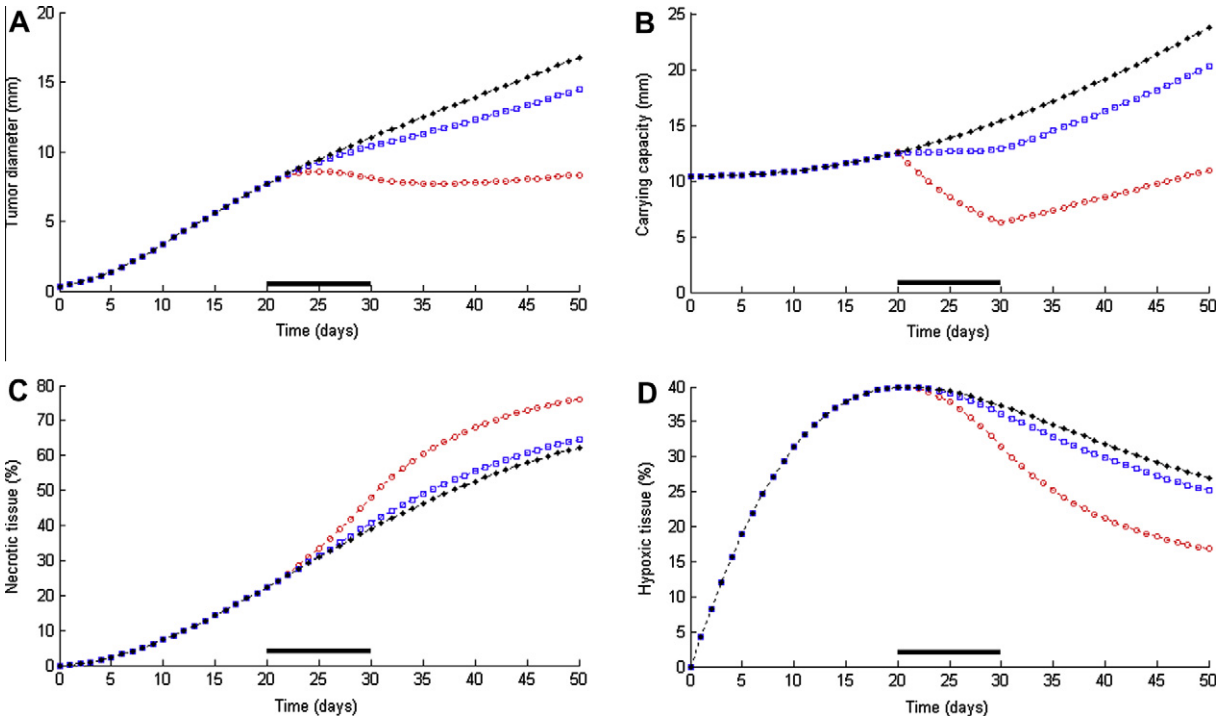

Fig. 5 – Simulation of antiangiogenic effect and comparison to tumour growth behaviour without treatment. We considered both 'vasculature inhibition' and 'vasculature disruption' effects. Simulations are performed using the mean estimated parameters for tumour growth behaviour. We simulated a 10-d treatment starting at day 20. In each image, the plain line with stars refers to the observed variable's behaviour without treatment, and the dashed lines with squares and circles refer to the same variable with 'vasculature inhibition' and 'vasculature disruption' treatments, respectively. (A) Evolution of tumour diameter. (B) Carrying capacity. (C) Necrotic tissue percentage. (D) Hypoxic tissue percentage.

studies. Furthermore, our results show that histological characteristics differ at different phases of tumour growth, suggesting that researchers should retrieve histological data at various times rather than at a single time point. It is worthwhile to note, however, that the model might be simplified to fit only tumour size data by 'merging' the different tissue compartments (P, Q and N) to one unique compartment (equivalent to P^*) and keeping as is the equation on the carrying capacity (K).

Finally, our model can serve as a basic tool to analyse tumour size and biomarker data for animals treated with antiangiogenesis therapy. In particular, the model could be further modified to include additional histological biomarkers such as density and diameter of intratumoural microvessels, which are traditionally used in the evaluation of antiangiogenic treatment. It would indeed be relevant to try to correlate the carrying capacity K with any combination of histological biomarkers related to blood vessels. Our model simulations predict that the two biomarkers we incorporated into the model - the percentage of hypoxic and necrotic tissues – might be indicative of the effect of antiangiogenic drugs. In particular, we predicted that tumours treated with antiangiogenic drugs may be characterised by a larger percentage of necrotic tissue and a lower percentage of hypoxic tissue in addition to a smaller size at the end of the treatment. Consequently, the percentages of necrotic and hypoxic tissues might be valid complementary candidates for biomarkers used in antiangiogenesis drug development. Further developments may also include coupling the model with relevant molecular biomarkers such as circulating VEGF and sVEGFR2.[25]

In the future, the model could be used to identify synergisms between conventional chemotherapy and antiangiogenic drugs and to investigate the effects of antiangiogenic agents on cytotoxic drug delivery. By understanding and monitoring the complex biological processes involved in vascular tumour growth, researchers will be able to quantify the beneficial effect of antiangiogenic drugs on chemotherapy delivery[26] and potentially streamline the delivery of these two medicines.

Like all attempts at modelling, our work on this complex model has limitations, some of which arise from the limited amount of data that were available. More data (a greater number of animals, different cell lines) would be needed to consolidate the analysis, in particular with regard to the analysis of histological biomarkers. As explained in the beginning of our paper, we chose to work with tumour diameter instead of using the classical ellipsoid approximation of tumour volume. This choice was motivated by numerous important considerations, but still, in this respect, our modelling results cannot be directly compared to those of modelling papers dealing with the analysis of tumour volume. As a consequence, some reservations may also be expressed regarding the model formulation itself. The model variables, which stand as quantities of tissues, are expressed in *mm*. From a physical point of view, as tumour tissues are composed of cells, it would

have been more consistent to deal with volume expressed in mm^3. Indeed, transfer of materials between the different types of tissues is likely to occur on three dimensions. This issue could be resolved by expressing all the model variables as volumes (mm^3) and taking the cube root of the output to compare to diameter observations. We note, however, that the use of ordinary differential equations (ODEs) to model a three-dimensional structure such as a tumour spheroid – where spatiality is clearly responsible for the organisation of tissue layers (necrotic at the core, proliferating at the periphery) – yields only a crude approximation of reality; in an ODE model, the use of volume data is not likely to provide a substantial improvement (if any) over the more abstract size representations incorporated into our model. Models incorporating partial differential equations are more suitable for addressing spatiality issues. Complex models describing the process of tumour angiogenesis integrate such equations,[9–12] and such model formulations have been successfully applied to the modelling of brain tumours, suggesting significant application potential in clinical settings.[27] In addition, the selection of mice for euthanasia may have introduced a statistical bias into the study. For ethical reasons, this selection was not random but based on objective and subjective criteria such as tumour size and the general behaviour of the mice. This bias mainly concerns the first animals selected and may thus have influenced the dynamic interpretation of the histological data. Tumour growth tended to be slower in the mice killed late compared with those euthanised early. This may have had consequences in the estimation of some model parameters as discussed in the Results section. Future studies should select animals for euthanasia at random while complying with ethical rules.

In conclusion, this study shows the first analysis of vascular tumour growth in mice combining tumour size and histological biomarkers. The integrated model contains four major components: non-hypoxic, hypoxic and necrotic compartments composing the tumour, as well as tumour carrying capacity, which changes according to tumour composition and eventually antiangiogenic drug effect. We show that the model can constitute a useful theoretical tool to investigate the efficacy of antiangiogenic drugs on tumour growth dynamics and composition.

Conflict of interest statement

None declared.

Acknowledgements

The authors wish to thank INSERM EMI 865 for kindly providing the HT29 and HCT116 cells. The help of Jean-Yves Scoazec, Colette Roche, Nicolas Gadot (ANIPATH) and Brigitte Tranchand is gratefully appreciated. We also thank France Mentré (INSERM EMI 0357), Marc Lavielle (INRIA Saclay – Île de France, project team SELECT) and the MONOLIX team (www.monolix.org) for valuable advice on model implementation, as well as Nick Holford (University of Auckland, NZ) for the diagnostic evaluation of the models. Jean-Pierre Boissel and Branka Bernard are acknowledged for valuable comments and Gianluca Satta and Alessandra Guadagno for their contribution to photos and preparation of figures.

REFERENCES

1. Folkman J. Role of angiogenesis in tumor growth and metastasis. *Semin Oncol* 2002;**29**:15–8 (6 Suppl. 16).
2. Jubb AM, Oates AJ, Holden S, Koeppen H. Predicting benefit from anti-angiogenic agents in malignancy. *Nat Rev Cancer* 2006;**6**(8):626–35.
3. Jain RK, Duda DG, Willett CG, et al. Biomarkers of response and resistance to antiangiogenic therapy. *Nat Rev Clin Oncol* 2009;**6**(6):327–38.
4. Simeoni M, Magni P, Cammia C, et al. Predictive pharmacokinetic–pharmacodynamic modeling of tumor growth kinetics in xenograft models after administration of anticancer agents. *Cancer Res* 2004;**64**(3):1094–101.
5. Magni P, Simeoni M, Poggesi I, Rocchetti M, De Nicolao G. A mathematical model to study the effects of drugs administration on tumor growth dynamics. *Math Biosci* 2006;**200**(2):127–51.
6. Rocchetti M, Simeoni M, Pesenti E, De Nicolao G, Poggesi I. Predicting the active doses in humans from animal studies: a novel approach in oncology. *Eur J Cancer* 2007;**43**(12):1862–8.
7. Wang Y, Sung C, Dartois C, et al. Elucidation of relationship between tumor size and survival in non-small-cell lung cancer patients can aid early decision making in drug development. *Clin Pharmacol Ther* 2009;**86**(2):167–74.
8. Claret L, Girard P, Hoff PM, et al. Model-based prediction of phase III overall survival in colorectal cancer on the basis of phase II tumor dynamics. *J Clin Oncol* 2009;**27**(25):4103–8.
9. Anderson AR, Chaplain MA. Continuous and discrete mathematical models of tumor-induced angiogenesis. *Bull Math Biol* 1998;**60**(5):857–99.
10. Scalerandi M, Sansone BC. Inhibition of vascularization in tumor growth. *Phys Rev Lett* 2002;**89**(21):218101.
11. Billy F, Ribba B, Saut O, et al. A pharmacologically based multiscale mathematical model of angiogenesis and its use in investigating the efficacy of a new cancer treatment strategy. *J Theor Biol* 2009;**260**(4):545–62.
12. Komarova NL, Mironov V. On the role of endothelial progenitor cells in tumor neovascularization. *J Theor Biol* 2005;**235**(3):338–49.
13. Hahnfeldt P, Panigrahy D, Folkman J, Hlatky L. Tumor development under angiogenic signaling: a dynamical theory of tumor growth, treatment response, and postvascular dormancy. *Cancer Res* 1999;**59**(19):4770–5.
14. Bueno L, de Alwis DP, Pitou C, et al. Semi-mechanistic modelling of the tumour growth inhibitory effects of LY2157299, a new type I receptor TGF-beta kinase antagonist, in mice. *Eur J Cancer* 2008;**44**(1):142–50.
15. Gorelik B, Ziv I, Shohat R, et al. Efficacy of weekly docetaxel and bevacizumab in mesenchymal chondrosarcoma: a new theranostic method combining xenografted biopsies with a mathematical model. *Cancer Res* 2008;**68**(21):9033–40.
16. Arakelyan L, Vainstein V, Agur Z. A computer algorithm describing the process of vessel formation and maturation, and its use for predicting the effects of anti-angiogenic and anti-maturation therapy on vascular tumor growth. *Angiogenesis* 2002;**5**(3):203–14.
17. Hansson EK, Houk B, Amantea M, et al. Pharmacokinetic–pharmacodynamic modelling of the angiogenic factors VEGF, sVEGFR-2, s-VEGFR-3 and skit following Sunitinib treatment in GIST. 2009, p. 18, Abstract 1521. Available from: <www.page-meeting.org/?abstract=1521>.

18. Tham LS, Wang L, Soo RA, et al. A pharmacodynamic model for the time course of tumor shrinkage by gemcitabine + carboplatin in non-small cell lung cancer patients. *Clin Cancer Res* 2008;**14**(13):4213–8.
19. Potter C, Harris AL. Hypoxic inducible carbonic anhydrase IX, marker of tumor hypoxia, survival and therapy target. *Cell Cycle* 2004;**3**(2):164–7.
20. Lindstrom ML, Bates DM. Nonlinear mixed effects models for repeated measures data. *Biometrics* 1990;**46**(3):673–87.
21. Samson A, Lavielle M, Mentre F. The SAEM algorithm for group comparison tests in longitudinal data analysis based on non-linear mixed-effects model. *Stat Med* 2007;**26**(27):4860–75.
22. Karlsson MO, Savic RM. Diagnosing model diagnostics. *Clin Pharmacol Ther* 2007;**82**(1):17–20.
23. Wilcoxon F. Individual comparison by ranking methods. *Biometrics* 1945;**1**:80–3.
24. Wählby U, Jonsson EN, Karlsson MO. Comparison of stepwise covariate model building strategies in population pharmacokinetic–pharmacodynamic analysis. *AAPS PharmSci* 2002;**4**(4):E27.
25. Duda DG, Ancukiewicz M, Jain RK. Biomarkers of antiangiogenic therapy: how do we move from candidate biomarkers to valid biomarkers? *J Clin Oncol* 2010;**28**(2):183–5.
26. Jain RK. Normalizing tumor vasculature with anti-angiogenic therapy: a new paradigm for combination therapy. *Nat Med* 2001;**7**(9):987–9.
27. Harpold HL, Alword Jr EC, Swansson KR. The evolution of mathematical modeling of glioma proliferation and invasion. *J Neuropathol Exp Neurol* 2007;**66**(1):1–9.